Control of Single Channel Conductance in the Outer Vestibule of the Kv2.1 Potassium Channel

Josef G. Trapani, Payam Andalib, Joseph F. Consiglio, and Stephen J. Korn

Department of Physiology and Neurobiology, University of Connecticut, Storrs, CT 06269

Current magnitude in Kv2.1 potassium channels is modulated by external [K^+]. In contrast to behavior expected from the change in electrochemical driving force, outward current through Kv2.1 channels becomes larger when extracellular [K^+] is increased within the physiological range. The mechanism that underlies this unusual property involves the opening of Kv2.1 channels into one of two different outer vestibule conformations, which are defined by their sensitivity to TEA. Channels that open into a TEA-sensitive conformation generate larger macroscopic currents, whereas channels that open into a TEA-insensitive conformation generate smaller macroscopic currents. At higher [K^+], more channels open into the TEA-sensitive conformation. In this manuscript, we examined the mechanism by which the conformational change produced a change in current magnitude. We started by testing the simplest hypothesis: that each pharmacologically defined channel conformation produces a different single channel conductance, one smaller and one larger, and that the [K^+]-dependent change in current magnitude reflects the [K^+]-dependent change in the percentage of channels that open into each of the two conformations. Using single channel and macroscopic recordings, as well as hidden Markov modeling, we were able to quantitatively account for [K^+]-dependent regulation of macroscopic current with this model. Combined with previously published work, these results support a model whereby an outer vestibule lysine interferes with K^+ flux through the channel, and that the [K^+]-dependent change in orientation of this lysine alters single channel conductance by changing the level of this interference. Moreover, these results provide an experimental example of single channel conductance being modulated at the outer end of the conduction pathway by a mechanism that involves channel activation into open states with different outer vestibule conformations.

The Journal of General Physiology

INTRODUCTION

Kv2.1 potassium channels are very slowly inactivating delayed rectifiers, found in a wide variety of neurons and nonneuronal excitable cells (Barry et al., 1995; Du et al., 1998; Murakoshi and Trimmer, 1999; MacDonald et al., 2001; Malin and Nerbonne, 2002; Muennich and Fyffe, 2004). Where its function in neurons has been examined, Kv2.1 appears to be responsible for repolarization of the action potential specifically during repetitive firing at frequencies of 1 Hz or more (Du et al., 2000; Malin and Nerbonne, 2002). Mechanistically, the relevance of Kv2.1 activity to repetitive firing may be associated with a distinctive channel function: the ability to have its current magnitude controlled in the face of changing external [K^+] (Wood and Korn, 2000; Andalib et al., 2002). This functional control of current magnitude is associated with an apparently unique, dynamic property of the channel's outer vestibule.

Kv2.1 channels display two distinct pharmacological profiles as a function of [K^+]: they can be either sensitive to external TEA with an IC50 of ~3–5 mM, or completely insensitive to TEA (Immke and Korn, 2000). Currents are larger and activate faster in TEA-sensitive channels, and smaller and more slowly activating in TEA-insensitive channels (Wood and Korn, 2000; Consiglio and Korn, 2004). This led to the hypothesis that [K^+]-dependent changes in macroscopic current magnitude result from a change in the percentage of channels that open into these two functionally distinct conformations. Additional evidence indicated that which of the two conformations a channel opens into is dependent on the occupancy, upon opening, of a single K^+ binding site within the conduction pathway (Immke et al., 1999; Immke and Korn, 2000).

The influence of outer vestibule conformation on current magnitude appears to be related to the orientation of outer vestibule lysine side chains with respect to the conduction pathway (these lysines are located at position 356, in the turret region of the channel; whether all four lysines are involved in a concerted reorientation or whether fewer than four lysines are involved is not known). In the conformation associated with smaller currents, the lysine side chains appear to be oriented more toward the center of the conduction pathway, where they interfere with the ability of K^+ to interact with an outer vestibule K^+ binding site (Immke et al., 1999; Immke and Korn, 2000; Consiglio et al., 2003). In the other conformation, which produces larger currents,

Correspondence to Josef Trapani: trapanij@ohsu.edu

Abbreviations used in this paper: HMM, hidden Markov modeling; Tet, tetracycline.

the lysine side chains apparently orient more away from the conduction pathway and interfere less with the outer vestibule K^+ binding site. For ease of communication, we will call these two conformations Lys_{in} and Lys_{out}, for conformations in which the lysine side chains are more toward the conduction pathway and more away from the conduction pathway, respectively.

In this manuscript, we address the mechanism by which lysine reorientation influences Kv2.1 current magnitude. Typically, modulation of current magnitude in voltage-gated channels occurs via an effect on gating. Whereas most studies of gating focus on the voltage-sensitive gate at the cytoplasmic entrance to the pore, there is a large body of evidence that also supports the possibility that the selectivity filter might play a role in activation gating (Chapman et al., 1997; Liu and Joho, 1998; Zheng and Sigworth, 1998; Perozo et al., 1999; Lu et al., 2001; VanDongen, 2004). Indeed, it is possible that gating at the selectivity filter underlies the final closed–open transition, which appears to be voltage independent (Schoppa and Sigworth, 1998; Zheng and Sigworth, 1998; Bao et al., 1999). The entire outer vestibule unit, from the turret through the pore helix to the internal TEA binding site, and up through the selectivity filter, is involved in the K^+-dependent change in conformation (see Immke et al., 1999). This widespread structural involvement that includes the selectivity filter makes a change in gating associated with the selectivity filter a plausible mechanism for modulation of current magnitude by the outer vestibule reorientation.

An alternative possibility is that the change in outer vestibule conformation alters current magnitude by causing a change in single channel conductance. This possibility represents our preferred hypothesis, based on the observation that the presence of lysine 356 (K356) reduces K^+ permeability by interfering with the outer vestibule K^+ binding site (Consiglio et al., 2003). However, there is little precedent for modulation of single channel conductance in voltage-gated channels. Mutation of residues at the outer entrance to the selectivity filter can influence single channel conductance (MacKinnon and Yellen, 1990; Haug et al., 2004), but a rational explanation for these effects is lacking. Thus, the possibility that Kv2.1 conductance is modulated by an outer vestibule mechanism would be unique in the literature in two respects: (1) that current magnitude in a voltage-gated channel could be physiologically regulated by modulation of single channel conductance and (2) that single channel conductance would be controlled by mechanisms within the outer vestibule of the channel.

In the present study, we examined these various hypotheses by combining single channel and macroscopic recordings, together with hidden Markov model analysis of very small conductance events. Our results demonstrate that there are two open channel conductance states in Kv2.1, one each associated with the Lys_{in} and Lys_{out} conformations. The observed magnitudes of the two conductances were consistent with the predicted influence of position 356 lysines on flux through the outer vestibule. Thus, our data indicate that changes in external $[K^+]$ alter macroscopic Kv2.1 current by changing the percentage of channels that open into each of the two outer vestibule conformations.

MATERIALS AND METHODS

Molecular Biology and Channel Expression

Experiments were done with the wild-type Kv2.1 channel and three mutant Kv2.1 channels, described in previous publications (Immke et al. 1999). Wild-type Kv2.1, a Kv2.1 channel in which two outer vestibule lysines were neutralized (Kv2.1 K356G K382V), and a Kv2.1 channel in which one of the two outer vestibule lysines was neutralized (Kv2.1 K356G), were studied in stably transfected CHO cells. For these experiments, channel expression was under the control of a tetracycline (Tet)-inducible promoter, so that expression levels could be controlled (see Trapani and Korn, 2003). For whole cell recordings, channel expression was initiated by incubating cells in 1 μg/ml tetracycline for 2 h on the day of recording. For single channel recordings, cells were maintained in Tet-free media (see below). Whole cell recording experiments in Fig. 3 used the two single mutation channels, Kv2.1 K356G and Kv2.1 K382V, subcloned into the pcDNA3 expression vector and expressed in HEK cells (see Andalib et al., 2002). Both CHO and HEK cells were maintained in Ham's F12 plus 10% FBS (Hyclone Laboratories, Inc.) with 1% penicillin/streptomycin. When HEK cells were used, cells were cotransfected by electroporation (Bio-Rad Laboratories Gene Pulser II at 220 V, 350 μF) with K^+ channel expression plasmid (0.5–10 μg/0.2 ml) and CD8 expression plasmid (0.5 μg/0.2 ml). After electroporation, cells were plated on glass coverslips submerged in maintenance media. Electrophysiological recordings were made 18–28 h later. On the day of recording, cells were washed with fresh media and incubated with Dynabeads M450 conjugated with antibody to CD8 (0.5 μl/ml; Dynal). Cells that expressed CD8 became coated with beads, which allowed visualization of transfected cells (Jurman et al., 1994). In the experiments of Fig. 3, as well as other types of experiments relevant to this study, channels expressed in HEK and CHO cells produced identical results (see Trapani and Korn, 2003).

Electrophysiology

Whole cell and single channel recording experiments were conducted at room temperature. Patch pipets for whole cell and single channel experiments were fabricated from N51A and 8250 glass, respectively (Garner Glass Co.), coated with Sylgard and fire polished. Currents were collected with either an Axopatch 1D (whole cell experiments) or an Axopatch 200B (both whole cell and single channel experiments) amplifier, pClamp 9 software, and a Digidata 1322A A/D board (Axon Instruments). Single channel currents were filtered at 1 kHz and sampled at 100 μs/pt for detection of larger (visibly observable) unitary events, and filtered at 2 kHz and sampled at 200 μs/pt for detection of hidden events (see below). Macroscopic currents were filtered at 2 kHz and sampled at 40–100 μs/pt. Series resistance ranged from 0.5 to 2.5 MΩ and was compensated 80–90%. In general, the maximum predicted series resistance error, after compensation, was ~2 mV. No corrections were made. The holding potential was −80 mV, and depolarizing stimuli were presented once every 10–60 s, depending on the experiment.

Data were analyzed with Clampfit 9 (Axon Instruments); curve fitting and significance testing (unpaired Student's t test) were done with SigmaPlot 8.0 (SPSS Inc.). All plotted data are represented as mean ± SEM. Differences between means were considered statistically significant if P values in unpaired Student's t tests were <0.05.

Single Channel Recording

Two issues had to be resolved in order to record single channel currents through Kv2.1 channels in a mammalian heterologous expression system. First, channel density had to be appropriately low for resolution of unitary events in a membrane patch. This was accomplished by using a CHO cell line in which channel protein expression was under the control of a Tet-inducible promoter. When cells were maintained in media made with Tet-free FBS, channel expression was reduced to a level that was suitable for single channel recording (Trapani and Korn, 2003). Moreover, endogenous K^+ channel expression is so low in CHO cells that recordings are not detectably contaminated by endogenous currents (Trapani and Korn, 2003).

A second issue is that Kv2.1 channels cannot be recorded in excised, inside-out patches due to rundown. In addition, our experience is that macroscopic Kv2.1 channel currents display a change in kinetic properties in outside-out patches (unpublished data). Consequently, we recorded single channel events in cell-attached patches. These experiments required that the membrane potential be known, and that both internal and external $[K^+]$ be controlled and known. To accomplish this, we used the procedure illustrated in Fig. 1 A. The pipet solution, which was the solution bathing the external face of the membrane patch, contained K^+ at a fixed concentration between 0 and 60 mM. Intracellular $[K^+]$ was maintained at a value that was identical to bath $[K^+]$ by including 30 μg/ml nystatin in the extracellular bathing solution. (In cell-attached patches, the "bath" solution is the extracellular solution bathing the entire cell except for the patch under the pipet, which is different from the "external" solution, which is the solution in the pipet that bathes just the outside of the patch.) Under these conditions, intracellular $[K^+]$ equilibrated with bath $[K^+]$, and changed as bath $[K^+]$ was changed (Horn 1991). Moreover, this equilibration maintained the cell membrane potential at 0 mV, so that the potential across the patch could be precisely known by controlling the pipet potential. Equilibration was complete within 3–4 min, as judged by changes in reversal potential (see below).

Fig. 1 (B–D) illustrates the utility and accuracy of this methodology. Fig. 1 B illustrates recordings of single channel currents from Kv2.1 K356G K382V at a series of membrane potentials, when both intracellular and external $[K^+]$ were 60 mM. As expected, currents reversed at 0 mV. Single channel current amplitudes were determined from all-points histograms. The four panels in Fig. 1 C illustrate I-V curves obtained from patches bathed in 60 mM external K^+ and four different concentrations of intracellular K^+. Each plot represents the averaged data from three or more cells. The graph in Fig. 1 D compares the observed reversal potentials (open circles) to those predicted by the Nernst equation (filled circles). This plot demonstrates that both membrane potential and intracellular $[K^+]$ were precisely controlled and known. Single channel conductances were determined from the slope of the I-V relationship over a specified voltage range. Data from individual patches were only used when a true reversal potential was within ±2 mV or an extrapolated reversal potential was within ±5 mV of that predicted by the Nernst equation.

As a control for these results with nystatin, we performed three other types of experiments. First, we changed bath $[K^+]$ in the absence of nystatin. Second, we changed intracellular $[K^+]$ in the presence of nystatin, and then removed the nystatin and changed the bath $[K^+]$. In both cases, the reversal potential deviated from that predicted from the Nernst equation (not depicted), presumably because the cell membrane potential, and possibly also intracellular $[K^+]$, were not known. Third, when bath $[K^+]$ was reduced without nystatin present (so that intracellular $[K^+]$ would not be expected to follow bath $[K^+]$), single channel currents did not display inward rectification as in Fig. 1 C.

Electrophysiological Solutions

Currents were recorded in a constantly flowing, gravity-fed bath. Solutions were changed in one of two ways. For most experiments, solutions were placed in one of six reservoirs, each of which fed via PE tubing into a perfusion manifold. Solution exited the manifold via a single quartz or PE tube. Cells were lifted off of the dish before recording and placed ~20 μm from the tip of the perfusion tube. One solution was always flowing, and solutions were switched manually (solution exchange was complete within 5–10 s). Faster solution changes were made as described previously (complete exchange when elevating concentration occurred within <20 ms; complete exchange upon reduction of concentration took slightly longer; Andalib et al., 2002). Except where noted in the figure legend, the intracellular solution in whole cell recordings contained (in mM) 100 KCl, 25 NMG-Cl, 10 HEPES, 10 EGTA, 1 $CaCl_2$, 4 $MgCl_2$; pH with NMG to 7.3, osmolality 290 mosm. Except where noted in the figure legend, the extracellular solution contained (in mM) 145 NMG-Cl, 10 HEPES, 10 glucose, 2 $CaCl_2$, and 1 $MgCl_2$; pH with NMG to 7.3, osmolality 330 mosm. For experiments in which drugs were added, if the drug concentration was <10 mM, drug was simply added to the external solution to the desired final concentration. If >10 mM drug was used, then it was substituted on an equimolar basis for NMG.

Single Channel Analysis

We studied two types of single channel events: directly visible (i.e., larger than background recording noise, which ranged from 0.09 to 0.12 pA rms; ~0.3–0.4 pA peak–peak) and hidden (i.e., signal to noise ratio was very small so that events were hidden within the recording noise). For the larger visible events, all points histograms (0.01 pA bin size) were created from the sum of 5–20 sweeps at a particular voltage. The histogram was adjusted such that the closed state peak was at 0 pA and outward currents (flux across the patch from the cytoplasm into the pipet) were positive. Histograms were fit to Gaussian distributions, and event magnitude was determined from histogram peaks (Clampfit 9).

Hidden events were analyzed using hidden Markov modeling (HMM). HMM analysis was performed by S.-H. Chung (Australian National University, Canberra, Australia). Dr. Chung was blind as to the experimental conditions and expected results of the supplied data traces. Details of algorithms used for HMM analysis can be found in Chung et al. (1990, 1991). The processing technique, which relies on the assumption that the noise is Gaussian and the signal sequence buried in the noise can be represented as a first-order Markov process, constructs maximum likelihood amplitude histograms to estimate the most likely signal sequence within the noise. Nonspecific anomalies in the noise were evaluated using FFT analysis. Our records occasionally contained a single peak at 120 Hz, which we could not eliminate. However, records obtained with channels closed (at −80 mV), and in untransfected cells, also displayed this 120-Hz peak in the noise but yielded no events in HMM histograms. Moreover, identical results were obtained in patches regardless of whether the 120-Hz peak was present.

For HMM analysis, 20 current traces (2-s duration each) were recorded at 0 and +40 mV. The 20 traces at a single membrane potential were concatenated to yield 40 s of single channel recording data, which was then analyzed. The concatenated record underwent 200 iterations of analysis to obtain the final current amplitude distribution. Each bin in HMM amplitude

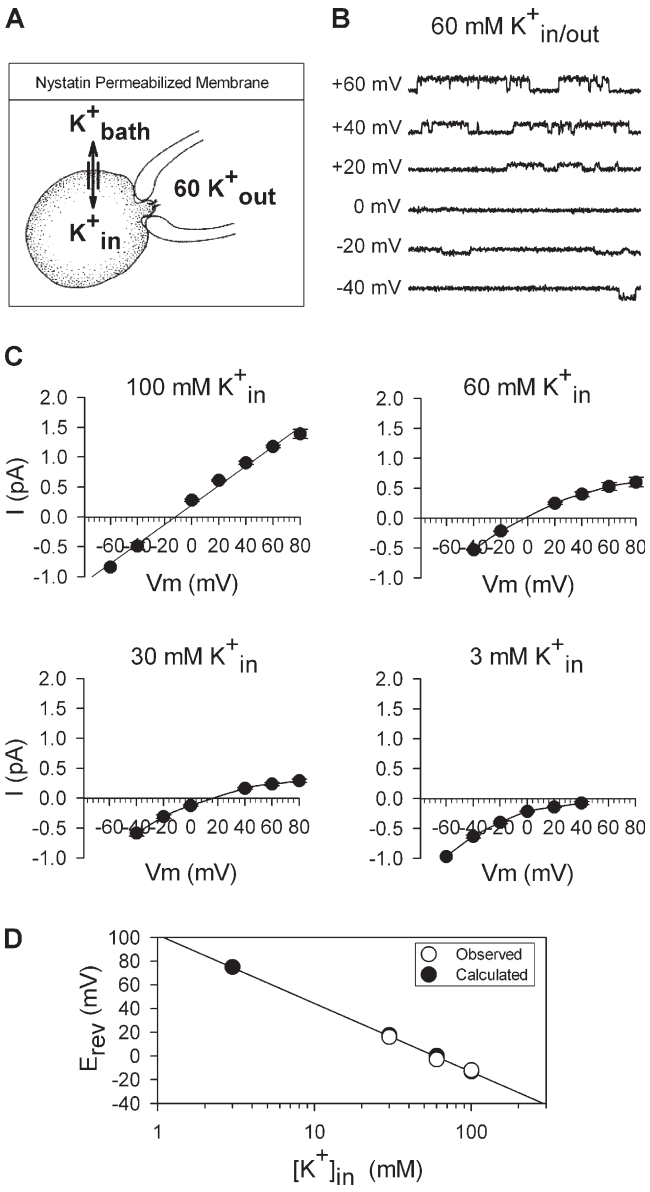

Figure 1. Method for recording single channel currents in cell-attached patches. (A) Cartoon of cell-attached patch configuration for recording single channel events. The extracellular bath solution (K^+_{bath}) contained 30 μM nystatin and the desired internal concentration of K^+ (K^+_{in}). The pipet solution was the external solution for the patch of membrane containing the channel to be studied, and contained 60 mM K^+. With nystatin in the membrane, K^+_{bath} and K^+_{in} equilibrated so that the internal concentration was the same as the bath concentration and the membrane potential, relative to the bath solution, was 0 mV. The potential across the membrane patch containing the channel being recorded was therefore set by the pipet potential. (B) Single channel recordings at a series of different membrane potentials with 60 mM internal and external K^+ to produce a reversal potential of 0 mV. Currents open upward at potentials positive to 0 mV and downwards at potentials negative to 0 mV. Single channel currents reversed at 0 mV. (C) Four panels illustrating I-V curves obtained from patches with 60 mM $[K^+]_{out}$ and four different K^+_{in}. Solid lines were drawn by hand. (D) Plot of observed reversal potentials (open circles) and those predicted by the Nernst equation (filled circles) for each $[K^+]_{in}$.

distribution histograms (e.g., Fig. 10) represented the fractional number of total digitized current measurements at a current amplitude. Thus, the peaks on the amplitude distribution histogram correspond to current magnitude of opening events, similar to the peaks on an all-points histogram. Histograms were divided into 100 bins, with a bin size that ranged from 0.005 to 0.015 pS, depending on the required resolution. The computer used for analysis was the Compaq AlphaServer SC at the Australian National University Supercomputer Facility, and it generally took ~30 min to 1 h to analyze a typical file, depending on its length.

RESULTS

As described in Introduction, elevation of external $[K^+]$ from 0 to 10 mM produces a concentration-dependent increase in outward current magnitude. At 0 mV, the $[K^+]$-dependent change in current magnitude reflects the functional consequence of the change in outer vestibule conformation (Andalib et al., 2002). Fig. 2 A illustrates the potentiation observed in CHO cells when external $[K^+]$ is elevated from 0 to 10 mM (intracellular $[K^+]$ = 100 mM). On average, current magnitude in CHO cells was increased by 34.6 ± 2.7% (n = 6), as compared with 38% in HEK cells (Wood and Korn, 2000; Andalib et al., 2002). Fig. 2 B illustrates a cartoon of the outer vestibule mechanism responsible for the change in current magnitude. In the "Lys_{in}" conformation, channels generate smaller currents and are TEA insensitive. In the "Lys_{out}" conformation, channels generate larger currents and are TEA sensitive. With 100 mM internal and 60 mM external $[K^+]$, all channels open into the Lys_{out} conformation (Immke and Korn, 2000). At external $[K^+] < 60$ mM, channels open into a mix of the two conformations; the percentage of channels in the Lys_{in} conformation increases as $[K^+]$ is reduced (Immke and Korn, 2000; Wood and Korn, 2000). Once activated by depolarization, channels remain in the conformation into which they open for the duration of the depolarizing pulse (Andalib et al., 2002). Consequently, when we wished to have all channels open in the Lys_{out} conformation, we activated channels in the presence of 60 mM external $[K^+]$ (all experiments described below were done with 100 mM internal K^+).

Macroscopic Conductance in the Wild Type and Lysine–substituted Kv2.1 Channels

The position 356 lysines (K356) reduce the ability of external K^+ to enter or leave the selectivity filter by interfering with an outer vestibule K^+ binding site (Consiglio et al., 2003). We extended these findings to different lysine mutation combinations so that we could quantitatively compare effects on macroscopic and unitary currents. To normalize macroscopic current magnitudes across cells, we used the area under the gating current as a measure of the number of channels being recorded (Consiglio et al., 2003). The top panels in

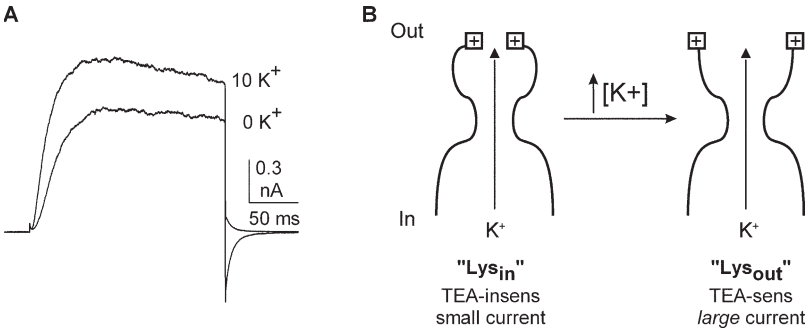

Figure 2. Outward K^+ current magnitude is potentiated by elevation of external $[K^+]$. (A) Outward K^+ currents through Kv2.1 channels in 0 and 10 mM K^+. Channels were held at −80 mV and depolarized to 0 mV for 200 ms. Note that the outward tail current was associated with 0 mM K^+ and the inward tail current was associated with 10 mM K^+. (B) Cartoon depicting the two outer vestibule conformations responsible for the increase in macroscopic current magnitude upon elevation of $[K^+]$. The left panel illustrates the Lys_{in} conformation, wherein the outer vestibule lysine (square with plus sign at outer edge of channel) is oriented toward the central axis of the conduction pathway. The right panel depicts the Lysout conformation, with the outer vestibule lysine oriented more away from the central axis of the pore.

Fig. 3 A illustrate gating currents from each of two channel types, recorded with 100 mM internal and external $[K^+]$ at 0 mV (the ionic current reversal potential). After recording the gating current from a cell, external $[K^+]$ was changed to 5 mM, and outward ionic currents were recorded at −20 mV (because gating current recordings required very high channel expression levels, ionic currents were recorded at −20 mV to keep ionic current magnitude reasonable). For a given size gating current, neutralization of the two outer vestibule lysines resulted in a larger macroscopic conductance (In Fig. 3 A, note that the activation kinetics of both gating and ionic currents are sensitive to $[K^+]$ via a mechanism that involves both K356 and the voltage sensor, and this effect accounts for the differences in kinetics observed in Fig. 3 A [Consiglio et al., 2003]. However, the G-V and Q-V curves for Kv2.1 and the double lysine mutant are identical and not influenced by $[K^+]$ [Wood and Korn, 2000; Consiglio et al., 2003]).

Fig. 3 B illustrates the normalized K^+ current magnitude, as obtained in Fig. 3 A, for the wild-type Kv2.1 channel, the double lysine mutant, and the two single lysine mutants. Macroscopic conductance in the double lysine mutant was 1.65-fold greater than that of the wild-type channel. As previously demonstrated for most other functional measures (Wood and Korn, 2000; Andalib et al., 2002; Consiglio et al., 2003), neutralization of the position 356 residue was entirely responsible for the change in macroscopic conductance observed in the double lysine mutant.

Single Channel Conductance in the Wild Type and Double Lysine Mutant Kv2.1 Channels

We next asked whether neutralization of the outer vestibule lysines in Kv2.1 produced a change in single channel conductance. Fig. 4 illustrates single channel records from the wild-type and double lysine mutant Kv2.1, recorded at +60 mV (traces below graph). The graph plots the complete I-V relationship for these two channels (filled and open circles, respectively) and also Kv2.1 with the single K356G mutation (filled diamonds). Currents were recorded with 100 mM internal and 60 mM external $[K^+]$ to ensure that all channels were in the Lys_{out} conformation. The I-V curves reversed at −13 mV (Kv2.1), −13.5 mV (Kv2.1 K356G K382V), and −13 mV (Kv2.1 K356G), which matched the predicted reversal potential of −13 mV for the targeted internal

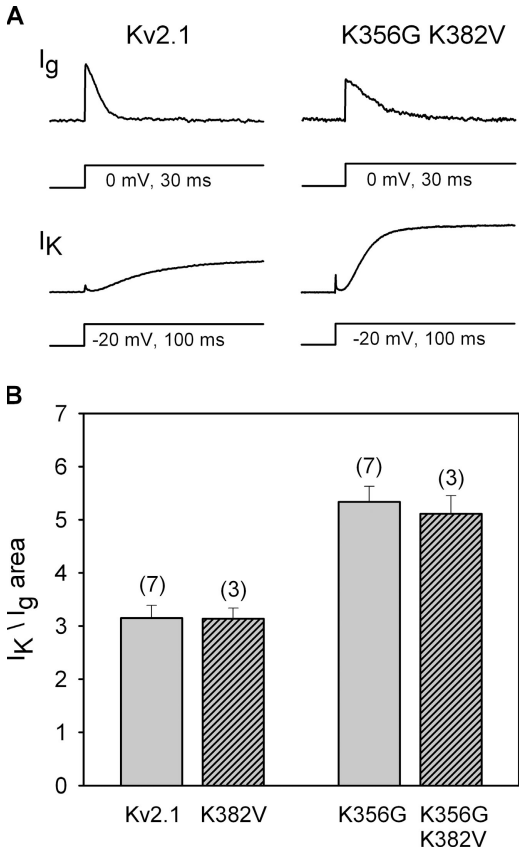

Figure 3. Neutralization of K356 caused a 65% increase in macroscopic conductance in 5 mM external K^+. (A, top) On-gating currents from each of two channel types (wt Kv2.1 and Kv2.1 K356G K382V) recorded at 0 mV (the ionic current reversal potential) with 100 mM symmetrical $[K^+]$. (A, bottom) After recording gating currents, external $[K^+]$ was changed to 5 mM to record outward ionic currents at −20 mV. (B) Ionic current magnitude, normalized to the area under the gating currents, for wt Kv2.1 and three mutant channels.

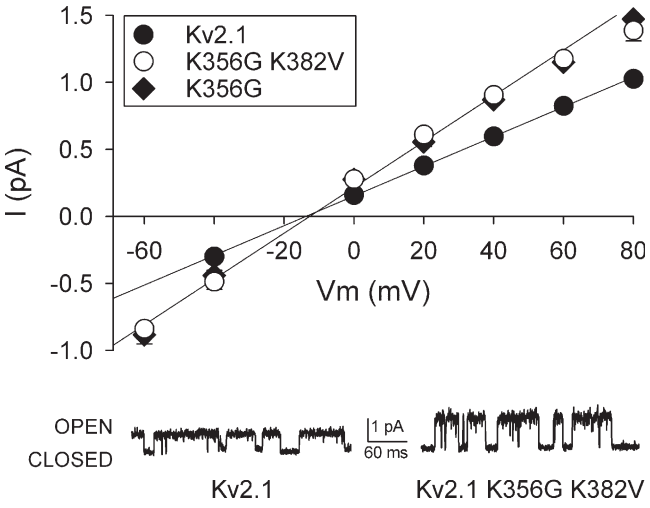

Figure 4. Neutralization of residue K356 increased single channel conductance by 60%. Main graph: I-V relationship for Kv2.1 (filled circles), the double lysine mutant (open circles), and the single K356G mutant (filled diamonds), obtained from single channel recordings. Current values at multiple membrane potentials were obtained with 100 mM internal and 60 mM external [K^+]. The lines represent the best fit of the data between −40 and +40 mV. Traces below graph: representative single channel records for the wild type and double lysine mutant channels, recorded at +60 mV.

and external [K^+]. Neutralization of the outer vestibule lysines resulted in an increased single channel conductance (note, however, that single channel currents still displayed just a single visible conductance state for each channel type). As observed with macroscopic current recordings, K356 was entirely responsible for the conductance difference. Single channel conductance, determined from the slope conductance measured between −40 and +40 mV, was 11.4 ± 0.2 pS (n = 3), 18.2 ± 0.7 pS (n = 3 – 4), and 17.4 ± 0.7 pS (n = 3) for Kv2.1, double mutant, and single mutant, respectively. Thus, with the outer vestibule in the Lys_{out} conformation, single channel conductance in the double lysine mutant was 1.6-fold greater than that of the wild-type channel. This closely matched the 1.65-fold increase observed in macroscopic recordings (Fig. 3).

Does Reorientation of K356 Influence Current Magnitude due to a Change in Single Channel Conductance?

Fig. 4 demonstrated that, with lysine residues at position 356 in the outer vestibule, single channel conductance was reduced. We next asked (a) whether reorientation of K356 from the Lys_{out} to the Lys_{in} conformation reduced single channel conductance further, and (b) whether such a change in single channel conductance could completely account for the observed [K^+]-dependent changes in macroscopic current magnitude (Fig. 2). To answer this question, we needed to determine both the single channel conductance of channels in the Lys_{in} conformation, and the percentage of channels in each conformation for a given [K^+]. However, direct observation of these single channel events is technically impossible for two reasons. First, in order to have a large percentage of channel openings into the Lys_{in} conformation, extracellular [K^+] needs to be near 0 mM, and intracellular [K^+] needs to be lowered to ∼10–30 mM (Immke and Korn, 2000). Given the already small single channel conductance of Kv2.1, single channel currents are too small to resolve at this low [K^+]. Second, at higher [K^+], we have never observed a second conductance state. As will be demonstrated below, channels in the Lys_{in} conformation generate a single channel current that is too small to identify visually, regardless of [K^+]. Consequently, we had to determine the conductance of the Lys_{in} conformation (g_{in}) indirectly. As will be seen below, the approach we used also produced a predicted percentage of channels in each of two conductance states.

The Indirect Approach To Determining Single Channel Conductance of the Lys_{in} Conformation at Different [K^+]

We calculated g_{in} indirectly from a combination of macroscopic conductance recordings and single channel recordings of channels in the Lys_{out} conformation. To calculate g_{in}, our approach first required determination of the single channel conductance of the Lys_{out} conformation (g_{out}) and the total number of channels in each conformation (N_{out} and N_{in}), for each [K^+]. Initially, we assumed there was no change in open probability (Po) at a given membrane potential, regardless of external [K^+] or the Kv2.1 channel being recorded. Five observations supported this assumption: (1) there was no change in the G-V relationship as a function of [K^+] (Wood and Korn, 2000), (2) there was no change in Q-V relationship as a function of [K^+] (Consiglio and Korn, 2004), (3) neutralization of K356 had no effect on the Q-V or G-V curves (unpublished data; Consiglio and Korn, 2004), (4) there was no apparent change in open–close flicker when the lysine was neutralized (see Fig. 4), and (5) the increases in macroscopic and single channel conductance upon neutralization of K356 are nearly identical (Figs. 3, 4). Given the assumption that Po remains constant at a given voltage, we arbitrarily set Po to 1 for each independent recording. This allowed us to simplify the expression, NPo (number of channels times Po) to N, and thereby simplify the notation in the equations (note that we could use any other value for Po and obtain the same results, as long as Po remains constant at a single membrane potential). To open channels, we depolarized the membrane to 0 mV. To measure macroscopic conductance, we applied 10-mV square voltage pulses (4 ms on, 6 ms off duty cycle) superimposed on the steady depolarization to 0 mV.

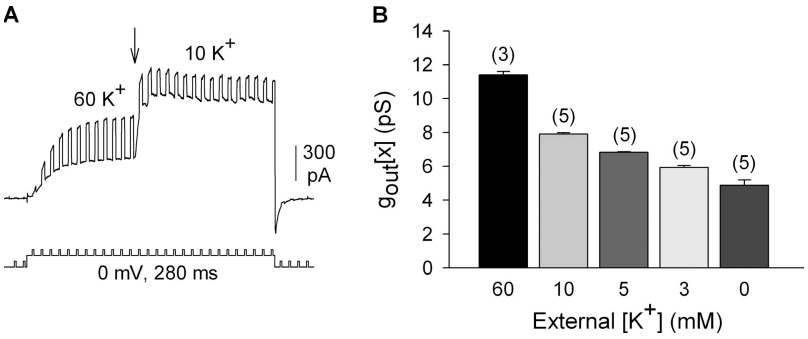

Figure 5. Indirect determination of single channel conductance for channels in the Lys_{out} conformation ($g_{out}[x]$). Macroscopic conductance was calculated by passing brief 10-mV voltage pulses superimposed upon the steady depolarization. (A) Cells were first activated in 60 mM K^+ so that all channels would open into the Lys_{out} conformation. At the arrow, external $[K^+]$ was rapidly switched to a new concentration (in this case 10 mM). For each cell, this protocol gave two macroscopic conductance values, $G_{tot}[60]$ (before the arrow) and $G_{tot}[x]$ (after the arrow). (B) Single channel conductance of the Lys_{out} conformation ($g_{out}[x]$) at different $[K^+]$. The value of $g_{out}[60]$ was obtained directly from single channel recordings (Fig. 4). The other values of $g_{out}[x]$ were calculated as described in the text.

Determination of g_{out} for Different External $[K^+]$

As discussed above, with 100 mM internal and 60 mM external $[K^+]$, all channels open into the Lys_{out} conformation (Immke and Korn, 2000). Therefore, we initially opened channels in 60 mM external $[K^+]$ to obtain a measure of total macroscopic conductance when all channels were in the Lys_{out} conformation ($G_{tot}[60]$; see Fig. 5 A, 60K). We next determined the total number of channels in the recording (N_{tot}) from

$$G_{tot}[60] = g_{out}[60] * N_{tot}, \quad (1)$$

where $g_{out}[60]$ is the measured unitary conductance of Lys_{out} channels obtained with 60 mM external $[K^+]$ (from Fig. 4). N_{tot} was determined for each individual cell.

Changes in external $[K^+]$ influence Kv2.1 channel conductance via two mechanisms: one mechanism that is associated with the change in outer vestibule conformation and one mechanism that is independent of this reorientation (Andalib et al., 2002). Consequently, we had to determine the single channel conductance for channels in the Lys_{out} conformation for each different $[K^+]$ ($g_{out}[x]$). To accomplish this, we took advantage of the fact that as long as the activating membrane potential is maintained, the outer vestibule conformation remains fixed even when external $[K^+]$ is changed (Andalib et al., 2002). Thus, if channels are initially activated in 60 mM external K^+, all channels will remain in the Lys_{out} conformation even after external $[K^+]$ is lowered. Experimentally after all channels were opened into the Lys_{out} conformation to obtain N_{tot} (see above), we changed external $[K^+]$ (Fig. 5 A, arrow) to measure $G_{tot}[x]$, the macroscopic conductance in the new $[K^+]$. We then calculated the value of g_{out} at the new $[K^+]$ from

$$G_{tot}[x] = g_{out}[x] * N_{tot}. \quad (2)$$

Fig. 5 A illustrates a recording from wild-type Kv2.1 channels used to obtain a value for $G_{tot}[10]$. Fig. 5 B illustrates a plot of $g_{out}[x]$ for a series of external $[K^+]$. The value shown for 60 mM K^+ was obtained directly from single channel recordings (see Fig. 4). The other values were calculated from the experiments described in Fig. 5 A and Eq. 2.

Comparison of Calculated g_{out} Values with Single Channel Measurements

To evaluate the ability of this approach to accurately determine $g_{out}[x]$, we obtained two additional single channel measurements, from two different channels. First, we measured single channel events for Kv2.1 with the external membrane bathed in 10 mM K^+ (Fig. 6, A and B). Single channel conductance, determined from the slope of the I-V curve, was 7.8 ± 0.3 pS (Fig. 6 B; $n = 3$). This was comparable to the calculated $g_{out}[10]$ value of 7.9 ± 0.1 pS (Fig. 5 B; $n = 5$).

We also compared calculated and measured single channel conductances for the double lysine mutant, Kv2.1 K356G K382V. We recorded single channel currents from Kv2.1 K356G K382V, in the presence of 5 mM external K^+ (Fig. 6, C and D). The measured single channel conductance at 5 mM K^+ ($g_{out}[5]$), determined from the slope of the I-V curve, was 10.3 ± 0.4 pS (Fig. 6 D; $n = 3$). Next, we calculated $g_{out}[x]$ from macroscopic currents, as described previously for wild-type Kv2.1. Initially, channels were opened in 60 mM external K^+ to obtain a measure of $G_{tot}[60]$ (Fig. 6 E). N_{tot} was then determined by dividing $G_{tot}[60]$ by 18.2, the measured single channel conductance in 60 mM external K^+ (from Fig. 4). While channels were activated, we changed external $[K^+]$ to 5 mM (Fig. 6 E, at arrow), and measured $G_{tot}[5]$. $G_{tot}[5]$ divided by N_{tot} gave a predicted $g_{out}[5]$ value of 10.2 ± 0.1 ($n = 5$).

These comparisons are summarized in Fig. 6 F. For the wild type and double mutant Kv2.1 channels, recorded with different external $[K^+]$, the $g_{out}[x]$ values calculated from macroscopic currents were essentially identical to the conductances measured in single channel recordings.

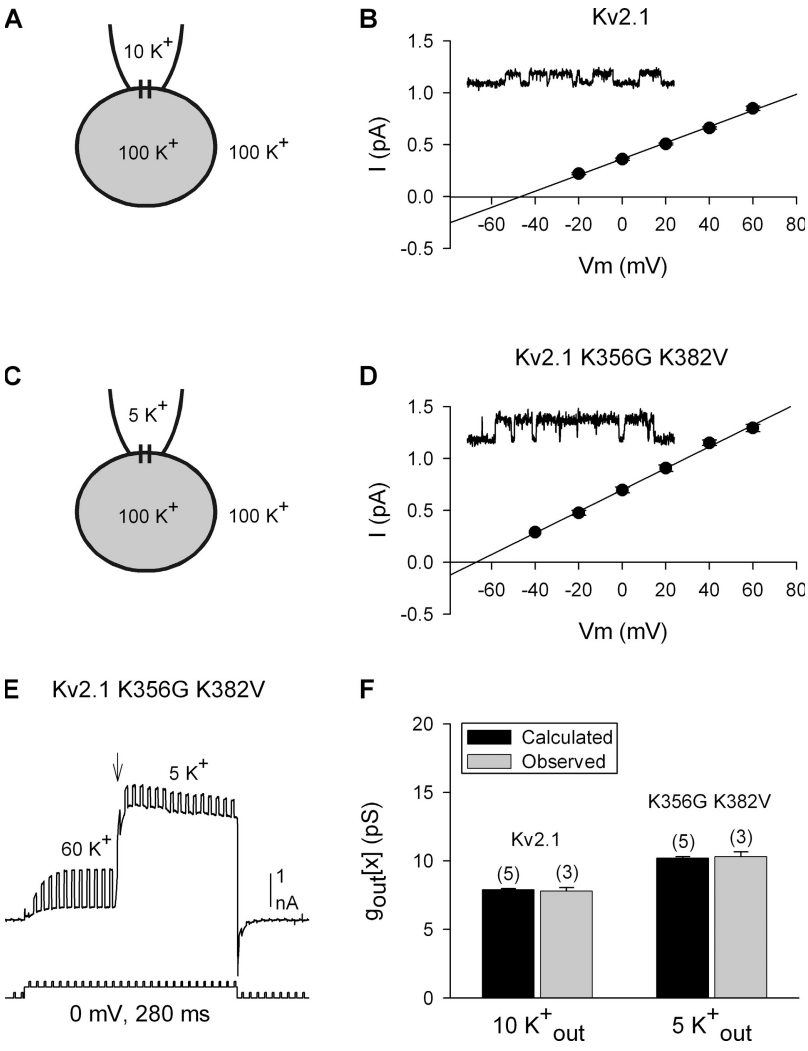

Figure 6. Comparison of calculated and directly measured $g_{out}[x]$. (A and C) Illustrations of the cell-attached patch setup and $[K^+]$ used for experiments described in B and D, respectively. (B) I-V relationship of single Kv2.1 channel currents recorded in 10 mM external K^+. The inset illustrates a representative trace at +60 mV. (D) Same as in B but for the mutant channel Kv2.1 K356G K382V. (E) Representative recording from the double mutant channel to obtain $G_{tot}[60]$ and $G_{tot}[x]$, as in Fig. 5. In this example, at the arrow, external $[K^+]$ was changed from 60 mM to 5 mM. (F) Comparison of single channel conductance values obtained from calculations (black bars) and direct measurements of unitary currents (gray bars) for Kv2.1 and the double lysine mutant.

Determination of Single Channel Conductance for the Lys_{in} Conformation (g_{in})

We now had a value for g_{out} at different $[K^+]$. In the next step, we calculated the single channel conductance of channels in the Lys_{in} conformation and the percentage of channels in the Lys_{in} and Lys_{out} conformations, for each $[K^+]$. To accomplish this, we used the ability of TEA to distinguish between channels in the two conformations. Channels in the Lys_{out} conformation are blocked by TEA, and those in the Lys_{in} conformation are not (Immke and Korn, 2000). First, we opened channels in the presence of 60 mM external $[K^+]$, so that all channels would be in the Lys_{out} conformation. We then blocked the current with 100 mM external TEA, which was previously shown to block currents by ~95% (Immke and Korn, 2000). As expected, 100 mM TEA blocked total channel conductance by 96.2 ± 0.1% (n = 16; Fig. 7 A). Because all channels were initially opened into the Lys_{out} conformation, the conductance that remained after TEA block reflected current through channels in the Lys_{out} conformation that were not blocked by 100 mM TEA (this lack of total block of Lys_{out} channels is merely a reflection of TEA potency; see Immke and Korn, 2000). The percentage of conductance not blocked by TEA directly translates into a percentage of Lys_{out} channels not blocked by TEA.

We now knew that ~4% of Lys_{out} channels were not blocked by 100 mM TEA (this initial block in high $[K^+]$ was repeated for each cell recorded, so that each cell had a measured percentage of unblocked Lys_{out} channels). Following this determination, TEA was removed and the original conductance in 60 mM K^+ completely recovered. Channels were then closed and reactivated in a different external $[K^+]$ (Fig. 7 B). Because they were closed and reactivated, channels could reopen into a different conformation (Andalib et al., 2002). Therefore, in the new, lower external $[K^+]$, the channel population opened into a mixture of Lys_{out} and Lys_{in} conformations (Andalib et al., 2002). We then reapplied 100 mM TEA in the presence of this new external $[K^+]$ (Fig. 7 B). Because TEA potency is unchanged by $[K^+]$ (Immke and Korn, 2000), we assumed that TEA blocked the same percentage of Lys_{out} channels

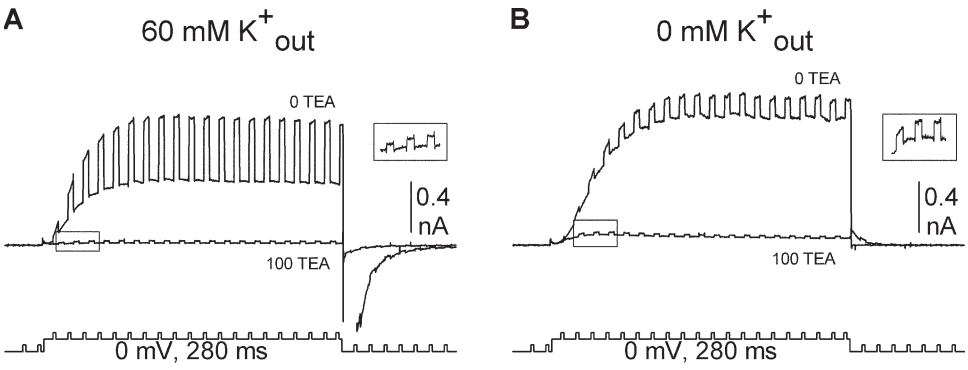

Figure 7. Determination of $G_{TEA\text{-}I}[x]$. (A) Channels were initially opened in 60 mM external K^+ to provide $G_{tot}[60]$. 100 mM TEA was applied and blocked the majority of channels. Because all channels open into the Lys_{out} conformation in 60 mM external K^+, the macroscopic conductance that remained after TEA application reflected the percentage of unblocked Lys_{out} channels. TEA was then removed and total conductance allowed to recover (not depicted). (B) In the same cell, channels were then opened in x mM external $[K^+]$ to provide $G_{tot}[x]$ (in this panel, x = 0 mM). 100 mM TEA was then applied in this subsaturating $[K^+]$. In this case, $G_{TEA\text{-}I}[x]$, the conductance remaining after TEA block, was composed of unblocked Lys_{out} channels plus all of the Lys_{in} channels. For clarity, the insets illustrate the boxed portion of the current recorded in 100 mM TEA in an expanded scale.

regardless of $[K^+]$ (i.e., in Fig. 7 (A and B), there was a different number of Lys_{out} channels, but the percentage of Lys_{out} channels not blocked remained the same). Therefore, the macroscopic conductance at this lower $[K^+]$ that was insensitive to 100 mM TEA ($G_{TEA\text{-}I}[x]$) reflected current through all of the Lys_{in} channels plus current through ~4% of the Lys_{out} channels present at this lower $[K^+]$.

From Eqs. 3–6 below, we were able to calculate the single channel conductance of the Lys_{in} channels, and the percentage of channels in each conformation, for different $[K^+]$. Fig. 7 B illustrates the measurement of the values needed for the evaluation of these equations. In this example, depolarization in 0 mM external K^+ yielded $G_{tot}[x]$, for x = 0. This conductance represented current through a mixture of Lys_{in} and Lys_{out} channels. Application of 100 mM TEA reduced conductance by 87.6 ± 0.3% ($n = 4$), leaving the total, TEA-insensitive conductance, $G_{TEA\text{-}I}[x]$. From Fig. 5 B, we knew $g_{out}[x]$. The total macroscopic conductance, $G_{tot}[x]$, is equal to the number of channels in each conformation times the single channel conductance for channels in each conformation (Eq. 3). As stated above, the total TEA-insensitive conductance, $G_{TEA\text{-}I}[x]$, is equal to the conductance contributed by all of the Lys_{in} channels plus ~4% of the Lys_{out} channels (Eq. 4; the value of 4% is illustrated for simplicity, but recall that this value was determined individually for each cell).

$$G_{tot}[x] = (N_{in}[x] * g_{in}[x]) + (N_{out}[x] * g_{out}[x]) \quad (3)$$

$$G_{TEA\text{-}I}[x] = (N_{in}[x] * g_{in}[x]) + (0.04 * N_{out}[x] * g_{out}[x]). \quad (4)$$

Subtraction of Eq. 4 from Eq. 3 yields

$$G_{tot}[x] - G_{TEA\text{-}I}[x] = (N_{out}[x] - 0.04 * N_{out}[x]) * g_{out}[x]$$

$$G_{tot}[x] - G_{TEA\text{-}I}[x] = 0.96 * N_{out}[x] * g_{out}[x]. \quad (5)$$

At this point, $G_{tot}[x]$, $G_{TEA\text{-}I}[x]$, and $g_{out}[x]$ are known. Therefore, we could determine $N_{out}[x]$ from Eq. 5 for each $[K^+]$. Using N_{tot}, calculated previously using Eq. 1, we determined $N_{in}[x]$ from

$$N_{in}[x] = N_{tot} - N_{out}[x]. \quad (6)$$

With $N_{out}[x]$, $N_{in}[x]$, and $g_{out}[x]$ determined, we solved Eq. 3 for $g_{in}[x]$.

For each $[K^+]$, we now have N_{tot}, N_{in}, N_{out}, g_{in}, and g_{out}. The values obtained for a series of $[K^+]$ are shown in Table I (the value for $g_{out}[60]$ was obtained directly from single channel recordings; Fig. 4).

Validity of the Calculated Data

The calculated data in Table I were derived from two types of measurements. First, $g_{out}[x]$ was determined by initially bathing cells in 60 mM external K^+ and then changing external $[K^+]$ to another value while channels were activated. Second, $g_{in}[x]$ and the number of channels in each conformation were derived in part from block of conductance by TEA. To check the validity of these numbers, we used them to predict conductance changes associated with a new set of experimental changes in $[K^+]$.

Table II compares experimentally observed to predicted changes in total macroscopic conductance (expressed as fold change) for changes in external $[K^+]$ from one concentration (x1) to another (x2). Predicted values were obtained by calculating $G_{tot}[x]$ from Eq. 3, using the values in Table I. Experimental results were obtained by measuring macroscopic conductance in one external $[K^+]$, and then again after closing and reopening channels in a different external $[K^+]$. Examples of conductance measurements for three different changes in $[K^+]$ are illustrated in Fig. 8. Without exception, there was excellent agreement between conductance

TABLE I

Kv2.1 Properties Predicted by Model

[x] mM	g_{in}[x] (pS)	g_{out}[x] (pS)	% Lys_{in}	% Lys_{out}
0	1.13 ± 0.02 (4)	4.88 ± 0.31 (5)	30.2 ± 0.8 (4)	69.8 ± 0.8 (4)
3	1.63 ± 0.08 (3)	5.93 ± 0.11 (5)	16.9 ± 0.8 (3)	83.1 ± 0.8 (3)
5	1.79 ± 0.06 (4)	6.82 ± 0.03 (5)	13.4 ± 0.7 (4)	86.6 ± 0.7 (4)
10	1.96 ± 0.12 (4)	7.90 ± 0.08 (5)	8.3 ± 0.6 (4)	91.7 ± 0.6 (4)
60		11.4 ± 0.2 (3)	0	100

TABLE II

Fold Change in Macroscopic Conductance

	[x1] mM	[x2] mM	Observed	Predicted
Fig. 8 B	0	3	1.40 ± 0.02 (8)	1.37
Fig. 8 A	0	10	1.94 ± 0.02 (6)	1.98
	0	60	3.07 ± 0.05 (8)	3.03
	3	10	1.42 ± 0.01 (8)	1.44
Fig. 8 C	3	60	2.20 ± 0.01 (8)	2.21
	5	10	1.20 ± 0.01 (4)	1.21
	5	60	1.86 ± 0.01 (4)	1.85
	10	60	1.54 ± 0.01 (8)	1.53

changes predicted by the values in Table I and the experimentally observed conductance changes.

Predicted Changes of Macroscopic Current

Our premise has been that the $[K^+]$-dependent alteration in current magnitude is fully accounted for by three mechanisms: (1) the change in single channel conductance that occurs independently of the change in outer vestibule conformation (e.g., changes in g_{out} at different $[K^+]$), (2) the change in macroscopic conductance associated with the transition of some channels between the small conductance (g_{in}[x]) and large conductance (g_{out}[x]) conformations, and (3) the change in electrochemical driving force. To test this, we used the values in Table I, together with the calculated change in driving force, to predict the $[K^+]$-dependent change in current magnitude. We then compared these predictions to experimental results. Three examples of experimentally obtained, $[K^+]$-dependent changes in current magnitude are illustrated in Fig. 9. The data in Table I predict that with a change from 10 to 60 mM external $[K^+]$, current magnitude at 0 mV will be reduced by 65.6%. In four cells tested as in Fig. 9 A, the change in external $[K^+]$ from 10 to 60 mM reduced peak current magnitude by 61.4 ± 1.0%. At 0 mV, the combined mechanistic contributions associated with more moderate changes in $[K^+]$ balance to produce little change in current magnitude (Andalib et al., 2002). Therefore, we conducted two additional tests at +50 mV. The values in Table I predict that a change in external $[K^+]$ from 3 to 10 mM will potentiate current measured at +50 mV by 12.5%. Experimentally, this change in external $[K^+]$ potentiated current by 11.7 ± 0.8% (n = 4; Fig. 9 B). The values in Table I predict that a change in external $[K^+]$ from 10 to 60 mM will reduce current magnitude at +50 mV by 11.7%. Experimentally, this change in $[K^+]$ reduced peak current by 11.3 ± 1.3% (n = 5, Fig. 9 C). Thus, the two different influences on conductance, quantified in Table I, combined with the expected change in driving force, fully account for the $[K^+]$-dependent change in current magnitude in Kv2.1.

HMM Analysis Detects Two Discrete Conductance States for Kv2.1 Channels

Given the hypothesis that there are just two functionally relevant outer vestibule conformations (with regard to open channel conductance), and the assumption that outer vestibule reorientation does not influence gating, the calculations above completely accounted for the observed $[K^+]$-dependent potentiation based on a difference in unitary conductance between the Lys_{in} and Lys_{out} conformations. However, this demonstration did not preclude the possibility that there are more than two conductance states, and although we believe the gating assumption to be well grounded, we had no direct evidence to support it. To test this hypothesis and assumption, we performed HMM analysis on current traces with potential hidden events. For Fig. 10, unitary Kv2.1 channels were recorded in 100 mM internal K^+ and 0 mM external K^+. At these concentrations, channels are predicted to open into the Lys_{in} state ~30% of the time (Table I). The observation of large conductance openings confirmed that channels were in the patch (Fig. 10 A). Large conductance events were

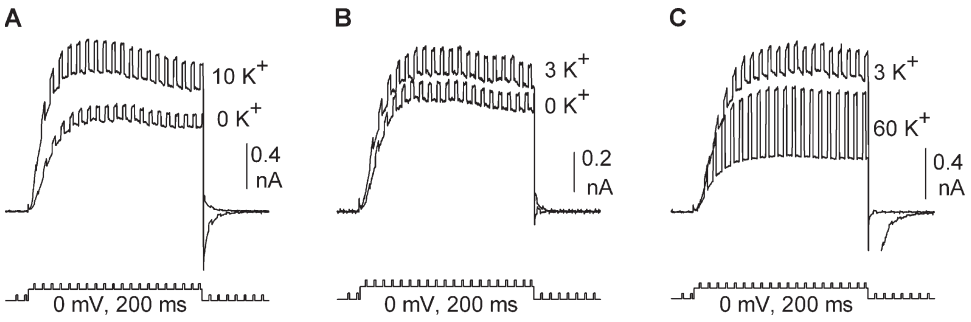

Figure 8. Measured potentiation of macroscopic conductance with elevation of $[K^+]$. (A) Channels were first opened in 0 mM K^+, closed, and reopened in 10 mM K^+. (B) Channels were first opened in 0 mM K^+, closed, and reopened in 3 mM K^+. (C) Channels were first opened in 3 mM K^+, closed, and reopened in 60 mM K^+.

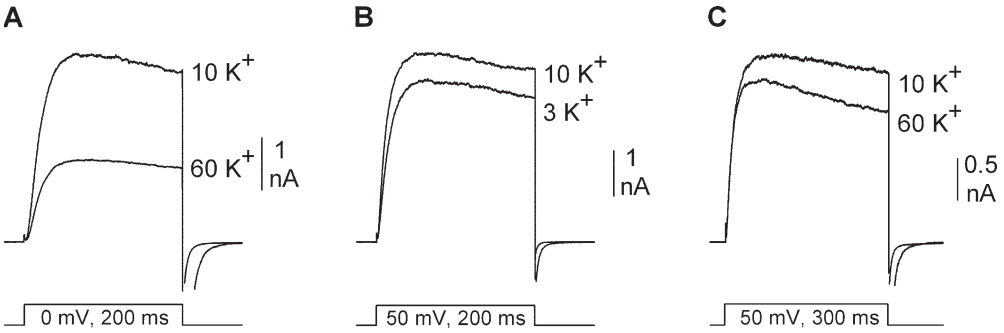

Figure 9. Measured changes in macroscopic currents with elevation of $[K^+]$. (A) Outward current was evoked in 10 mM external $[K^+]$ by depolarization to 0 mV. Channels were then closed and reopened in 60 mM $[K^+]$. (B) Same as in A except that currents were recorded at +50 mV and external $[K^+]$ was changed from 3 to 10 mM. (C) Same as in B except that external $[K^+]$ was changed from 10 to 60 mM.

analyzed in two different ways. First, standard amplitude histograms were created from measurement of observed events at multiple potentials. The best fit slope of the I-V relationship for observed, large conductance (Lys_{out}) events was 5.6 ± 0.5 pS ($n = 3$), which agreed well with 4.9 ± 0.3 pS from Table I (compare solid with dashed line in Fig. 10 A). Second, traces collected at 0 mV (Fig. 10 A) were analyzed using the HMM algorithm. HMM analysis found two current levels (Fig. 10 D). One level was the closed or 0 current level, and one had a unitary current of 0.38 pA (arrow), which was identical in magnitude to the direct measurement of the observed openings (Fig. 10 C).

To detect potential smaller, hidden channel conductance events within the noise of concatenated traces, it was necessary to focus the algorithm on a specific current range. To exclude the larger events from the analysis, cursors were set to detect events between ± 0.375 pA and the signal divided into 100 equal sized bins (0.0075 pA each). Portions of the record that included large conductance openings (Fig. 10 A) were excluded from the concatenated record before analysis (see Materials and Methods). Fig. 10 (E and F) illustrates HMM histogram results for recordings made at 0 and +40 mV (bin size for the +40 mV recording was set to 0.005 pA). In each case, two peak current levels were observed. In addition to the histogram peak at the closed or 0 current level, peak current levels (arrows) were observed at 0.075 pA and 0.12 pA, for recordings at 0 and +40 mV, respectively. The slope conductance from these values (Fig. 10 B, gray symbols) was 1.13 pS, which was identical to the calculated g_{in} value from Table I.

We repeated this analysis for another set of $[K^+]$. HMM analysis of data collected in 100 mM internal and 10 mM external K^+, at +40 mV, revealed two current levels in addition to the closed, 0 current level. The directly observed larger openings (also detected by HMM analysis) had an average current magnitude of 0.62 ± 0.1 pA ($n = 3$; Fig. 11 A, black bar). The smaller events, detected by HMM analysis of the same patches, yielded a peak current level of 0.16 ± 0.2 pA (Fig.11 A, gray bar). Thus, the current magnitude of the hidden events was 25.7 ± 3.6% ($n = 3$) that of the larger events. Fig. 11 B compares two experimentally determined small event/large event (i.e., Lys_{in}/Lys_{out}) conductance ratios to those calculated in Table I. The black bar at 0 mM K^+ represents the experimentally determined conductance ratio obtained from the slope conductances in Fig. 10 B. The hatched black bar represents the experimentally determined ratio from the data in Fig. 11 A. The gray bars represent ratios calculated from Table I, which reflect the results of our indirect approach to calculating Lys_{out} and Lys_{in} values. The conductance ratios obtained from HMM are in good agreement with the ratios obtained by our indirect approach. The results of Figs. 10 and 11 strongly support the hypothesis that there are two discrete conductance states, one each that would correspond to the Lys_{out} and Lys_{in} conformations. Moreover, the quantitative accounting of these two conductance states, detected by observation and HMM analysis, for the $[K^+]$-dependent potentiation, validates the assumption that a change in gating does not play a role in the potentiation.

Finally, HMM analysis of currents recorded in 100 mM internal and 60 mM external K^+ failed to detect any events other than those corresponding to the closed, 0 current level and a large, directly observable current level (unpublished data). These results are consistent with the previous results that at 60 mM K^+, all channels are in a single conformation (the larger Lys_{out} conformation). Moreover, this experiment serves as a negative control that supports the interpretation that the very small events detected by HMM analysis at lower $[K^+]_{out}$ represented currents through the Lys_{in} conformation.

DISCUSSION

We previously demonstrated that Kv2.1 channels can open into one of two conformations, one TEA sensitive and one TEA insensitive (Immke and Korn, 2000). Which conformation Kv2.1 channels open into is determined by the interaction of K^+ with a single selectivity filter binding site (Immke et al., 1999; Immke and Korn, 2000). At higher $[K^+]$, more channels open with this

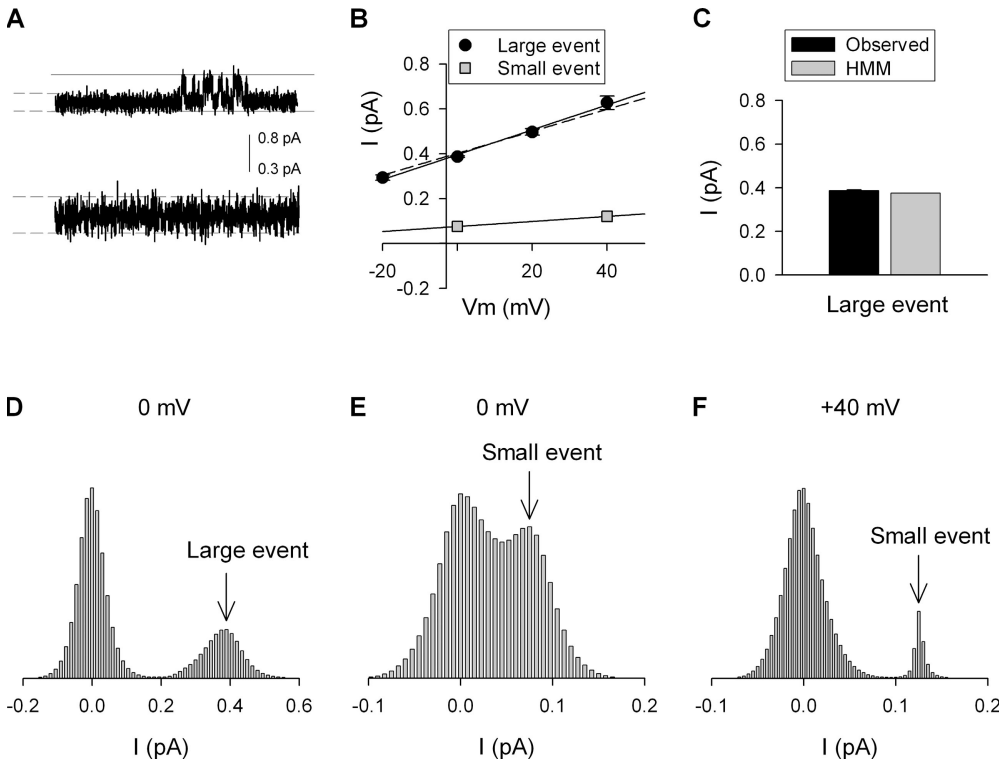

Figure 10. HMM analysis of single channel recordings in 0 mM external $[K^+]$. (A, top) Representative current trace (600 ms duration) from a recording at 0 mV. Channel openings are illustrated as going in the upward direction. The solid horizontal lines are placed 0.8 pA apart and correspond to the histogram limits (see D) for detection of the large visible event with HMM. (A, bottom) The initial 300 ms of the upper trace is expanded to illustrate with higher resolution the noise, which might contain small hidden events. The dashed lines correspond to the histogram limits (see E and F) for detection of hidden small events. (B) I-V plots of the large directly observed events (black circles) and HMM detected small hidden events (gray squares; from histograms in E and F). The data from large events were best fit with a slope conductance of 5.55 ± 0.48 pS (solid line), which compares well with the calculated value for the Lys_{out} conformation (dashed line; Table I). The data from small hidden events were best fit by a line with a slope conductance of 1.13, which is identical to that predicted in Table I. (C) Comparison of the current magnitude of large events, recorded in 0 mM external K^+, determined from direct measurement of unitary events (black bar) and HMM detection of large unitary events (gray bar). (D) Histogram generated by HMM analysis of concatenated traces including portion shown in A (top). Two peaks were found: the peak at 0 pA corresponded to the channel closed current level, the peak (arrow) at 0.38 pA corresponded to the amplitude of the large events (Lys_{out}). Note that small state events were potentially present but hidden within the large 0 pA histogram peak. (E) To perform HMM analysis with higher resolution, the noisy portion of the entire concatenated record was expanded (see lower part of A), boundary cursors were placed as shown in dashed lines in A, and the large visible opening events were deleted from the record. HMM analysis yielded a histogram with a peak at 0.075 pA (arrow) corresponding to the small hidden events. (F) Same as in E but channel activity was recorded at +40 mV. HMM analysis detected small hidden events with an average current level of 0.12 pA (arrow).

regulatory site occupied, and consequently, more channels open in the Lys_{out} conformation. At lower $[K^+]$, the probability that this site will be occupied upon channel opening is decreased. Channels that open with this site unoccupied open into the Lys_{in} conformation. At physiological $[K^+]$, once channels are activated by depolarization, the outer vestibule conformation remains fixed even if external $[K^+]$ changes (Andalib et al., 2002). However, once channels deactivate, they may reopen into a different conformation (Andalib et al., 2002). This ability of the outer vestibule to change conformation allows Kv2.1 current magnitude to be modulated by physiologically relevant changes in external $[K^+]$ (Immke and Korn, 2000; Wood and Korn, 2000).

A wide range of evidence strongly supports a model whereby the functional consequences of the change in outer vestibule conformation result from a change in orientation of a single outer vestibule lysine (K356) relative to the central core of the conduction pathway (Immke et al., 1999; Immke and Korn, 2000; Wood and Korn, 2000; Andalib et al., 2002; Consiglio and Korn, 2004). K356 also interferes with the interaction of K^+ with an outer vestibule K^+ binding site, regardless of outer vestibule conformation (Consiglio et al., 2003). One consequence of this interference is a reduction of K^+ flux through the pore (Consiglio et al., 2003). Consequently, a simple mechanistic model emerged whereby the reorientation of K356 toward the central axis of the conduction pathway increased this interference and thus reduced current magnitude even more. The simplest possible model was one in which there were just two conductance states, one each associated with the Lys_{in} and Lys_{out} conformations. Thus, if channels opened with the lysine oriented more toward the central axis of the conduction pathway, single channel conductance would be reduced. If channels opened with the lysine oriented more away from the central axis, single channel conductance would be greater.

An alternative possibility, however, would be that the change in outer vestibule conformation might influence current magnitude by altering channel open probability. There is much evidence, albeit indirect and

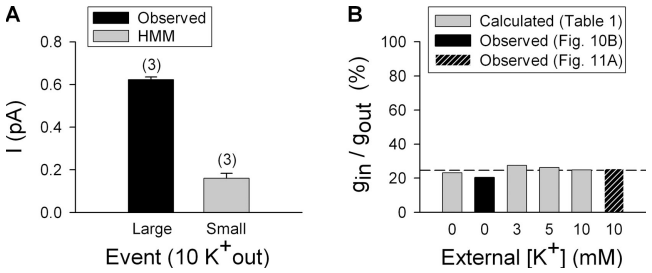

Figure 11. Conductance ratio of small and large conductance events. (A) Single channel current magnitude was determined with 10 mM external $[K^+]$ at +40 mV. The black bar plots the current magnitude of large, directly observed unitary events. The gray bar plots the current magnitude of small, hidden events detected by HMM analysis. (B) Graph of conductance ratios at different external $[K^+]$. Gray bars plot the ratio obtained from the calculated values in Table I. The black bar plots the ratio obtained from the experimentally obtained slope conductances in Fig. 10 B. The hatched bar plots the experimentally obtained ratio from A of this figure.

circumstantial, that protein fluctuations at the selectivity filter underlie closed–open transitions associated with activation gating (see Introduction). The conformational change reorients not only the outer vestibule turret but also residues just internal to the selectivity filter (Immke et al., 1999). Indeed, it appears that the conformational change involves the entire P-loop region of the channel, which extends from the outer vestibule through the selectivity filter to the inner vestibule at the level of the internal TEA binding site. It is reasonable, therefore, to suspect that this wide-ranging conformational change could influence fluctuations at the selectivity filter.

The results described in this manuscript provide strong evidence for the hypothesis that outer vestibule reorientation exclusively alters single channel conductance, and that there are just two conductance states, one each associated with the Lys_{in} and Lys_{out} conformation. The change in Kv2.1 current magnitude associated with changes in $[K^+]$ are completely accounted for by a change in the percentage of channels that open into each conformation at different $[K^+]$. At higher $[K^+]$, more channels open into the higher conductance, Lys_{out} conformation, and macroscopic currents are consequently larger. At lower $[K^+]$, a larger percentage of channels open into the lower conductance, Lys_{in} conformation, and macroscopic currents are smaller.

Use of Three Independent Techniques To Obtain the Desired Quantitative Results

In an ideal world, what one would want to do to address this problem would be to measure single channel conductances and gating kinetics associated with each channel state. This was not possible in this study for at least two reasons. First, we could only detect the small conductance state with HMM analysis. In principle, HMM can both identify single events of different conductance with great resolution and also analyze gating kinetics. However, we could never know how many channels were in a recording, which made analysis of gating kinetics impossible. Second, we required single channel conductance measurements at low $[K^+]$. At many of the required $[K^+]$, even currents through the large conductance state, as well as through the small conductance state, would be too small to measure.

To get around these obstacles, we combined three independent methods. We created a simple model based on the hypothesis that $[K^+]$-dependent changes in current magnitude could be accounted for entirely by changes in single channel conductance. This was well grounded in the experimental observation that the presence of the lysine at position 356 reduced conductance (Consiglio et al., 2003; Trapani and Korn, 2003). We then used macroscopic and single channel conductance measurements to determine the large conductance magnitude, and consequently predict the small conductance magnitude and percent of channels in each conductance state, that would produce the observed $[K^+]$-dependent change in macroscopic current. This approach depended critically on having a drug, TEA, that was absolutely selective for blockade of one, but not the other, conductance state. We then used HMM analysis for a limited but critical purpose: to test the hypothesis that there were only two conductance states, and to determine whether the predicted magnitude of the small conductance state was accurate. The confirmation via HMM analysis that there were just two conductance states supported the validity of the initial simple model. The confirmation via HMM that the conductance magnitudes predicted by the model were accurate supported the conclusion that the solutions of the model, derived in part from direct experimental measurement and in part from prediction, were unique. Moreover, the close match between experimentally determined and predicted conductances over a range of $[K^+]$ provided strong support that this model accounted for the $[K^+]$-dependent change in current magnitude.

Validation of Assumptions

The calculations of single channel conductances and number of channels in each conformation at a given $[K^+]$, derived from macroscopic and some key single channel recordings, depended critically on two assumptions: (1) that there were just two different open conductance levels and (2) that the $[K^+]$-dependent change in current magnitude did not result from a change in open probability. The rationale underlying these assumptions was described earlier in the manuscript. We used HMM analysis to detect hidden events for the very specific purpose of validating and/or testing these assumptions. First, at subsaturating $[K^+]$, HMM revealed exactly two discrete open conductance states. At 60 mM

external K^+, in which all channels open into the Lys_{out} conformation, HMM analysis revealed just one open conductance state, which corresponded with the larger, Lys_{out} conductance. These observations support the model in which each conformation, defined by TEA sensitivity, was associated with just one single channel conductance. Second, the magnitude of the single channel conductances (of both larger and smaller events) revealed by HMM analysis were quantitatively identical to those calculated based on the assumptions (Table I). The precise match of HMM-detected and calculated conductances could only result if both assumptions, that there were just two conductance states and that Po was unchanged by the change in conformation, were valid.

Comparison of Predicted and Experimental Differences between Kv2.1 and the Double Lysine Mutant

Neutralization of both outer vestibule lysines produced a 1.65-fold increase in conductance in macroscopic recordings (Fig. 3) and a 1.60-fold increase in conductance in single channel recordings. Although these values would seem to compare reasonably well, we knew that the two measurements were made under slightly different conditions. The macroscopic measurements were made in the presence of 5 mM external K^+, which results in a small percentage of Kv2.1 channels opening into the Lys_{in} conformation (Immke and Korn, 2000; Table I). In contrast, the single channel measurements were made exclusively from Kv2.1 channels in the Lys_{out} conformation. Consequently, we asked whether the slight discrepancy in conductance ratios (1.65 vs. 1.60-fold increase in conductance) obtained from macroscopic (Fig. 3) and single channel (Fig. 4) recordings was due to the inclusion of a small percentage of channels in the Lys_{in} conformation in the macroscopic but not the single channel recordings.

For the double lysine mutant, the single channel conductance at 5 mM K^+ is 10.2 pS (Fig. 6; note that there is only one conductance value, as conductance in the double lysine mutant is unaffected by outer vestibule conformation [Andalib et al., 2002]). So, for example, macroscopic conductance for 100 channels would be 1020 pS. At 5 mM K^+, the macroscopic conductance for wild-type Kv2.1 would be composed of 86.6% of channels with a single channel conductance of 6.82 pS and 13.4% of channels with a single channel conductance of 1.79 pS. For 100 channels, the macroscopic conductance would be 614.6 pS. Thus, using the values in Table I for 5 mM external K^+, the macroscopic conductance of the double lysine mutant will be 1.66 times that of wild-type Kv2.1. This value is essentially identical to the 1.65-fold difference obtained experimentally (Fig. 3). Indeed, we'd be surprised if our experimental approach had the resolution to detect this small difference. However, we found it to be of some value that, indeed, the experimental results comparing potentiation between two channels were predicted quite accurately by the model.

Where Is Conductance Regulated in K^+ Channels?

Theories of single channel conductance have sought to identify a uniform mechanism by which ion channels generate high conductances with high selectivity. More than any other channel type, K^+ channels display a wide range of single channel conductances, so any permeation theory should account for an ability to vary conductance considerably using quite similar molecular structures. Perhaps ideally, a universally applicable theory would identify a common event, such as ion exit, ion entry, or passage through the narrowest region of the pore, as rate limiting for flux in all channels. Accumulating evidence, however, is now casting doubt on the existence of a single location, or mechanism, of conductance limitation.

The potential role of the selectivity filter in determination of conductance is unresolved. The selectivity filter is the narrowest region of the pore, where K^+ is known to bind with highest affinity. This makes the selectivity filter an intuitively attractive location to determine flux rate through the channel. Indeed, mutation at or near the selectivity filter can alter single channel conductance (Lu et al., 2001; So et al., 2001). However, selectivity filter mutagenesis is often accompanied by changes in selectivity (Taglialatela et al., 1993; Chapman et al., 2001; Lu et al., 2001), so that conductance changes may be associated with meaningful changes in selectivity filter operation. Moreover, the near identity of primary sequence and quantitative similarity of selectivity in different channels, despite a wide range of single channel conductance values (from 2 to several hundred picoSiemens), provides a significant complication to the proposal that conduction variation is associated with differences in the selectivity filter. Indeed, recent theoretical and structural studies have proposed that the selectivity filter region is most likely designed for extremely high throughput (Bernèche and Roux, 2001; Morais-Cabral et al., 2001). Nonetheless, structurally similar selectivity filters may behave quite differently. For example, whereas the KcsA selectivity filter appears to be fully occupied at physiological [K^+], the Kv2.1 selectivity filter appears to be incompletely occupied at physiological [K^+] (Korn and Trapani, 2005).

Recently, structural, theoretical, and molecular data have shifted the focus of permeation theory toward the inner vestibule. Using structural data from the KcsA channel, Chung et al. (2002) showed, via Brownian dynamics simulations, that single channel conductance could be altered by subtle changes in diameter of the intracellular entrance. Subsequently, experimental studies of both KcsA and the Ca^{2+}-dependent potassium channel, BK, demonstrated that the large differences in

single channel conductance between BK channels and smaller conductance K^+ channels were likely due, at least in part, to structural differences in the internal entrance to the pore (Brelidze et al., 2003; Nimigean et al., 2003). In support of these findings, accessibility studies with large quaternary ammonium compounds described an enlarged inner vestibule in the large conductance, Ca^{2+}-dependent K^+ channel, as compared with other K^+ channels (Li and Aldrich, 2004). Similarly, Brelidze and Magleby (2005), who used sugar molecules as probes of inner vestibule access and geometry, described how a wide inner vestibule entrance was necessary for BK's large conductance. Thus, it appears that the extremely high conductance associated with BK is largely, if not exclusively, associated with a high rate of K^+ entry into the inner vestibule.

For Kv2.1, the Outer Vestibule Is Important

In this manuscript, we demonstrated that the presence of a single lysine in the outer vestibule in Kv2.1 reduces single channel conductance by 40% (Fig. 4). Most importantly, Kv2.1 channels can open with this lysine oriented in two different ways, depending on the association of K^+ with a particular K^+ binding site in the pore (Immke and Korn 2000). Channels that open into one conformation, which we have called the Lys_{in} conformation, have a single channel conductance that is ~75% smaller than channels that open into the Lys_{out} conformation. Under physiological conditions, changes in external $[K^+]$ between 3 and 30 mM change the percentage of channels in each conformation, so that at higher $[K^+]$, more channels open into the larger conductance state (see Immke and Korn, 2000, for concentration dependence). These studies demonstrate, for the first time that we know of, that single channel conductance in at least one voltage-gated K^+ channel is modulated by a physiologically relevant event, and that the mechanism that underlies this modulation occurs in the outer vestibule.

Physiological Relevance of K^+-dependent Modulation of Conductance

Despite a widespread expression throughout the mammalian brain, the precise physiological role of Kv2.1 channels in most regions is not known. In hippocampal neurons, Kv2.1 is highly expressed (Murakoshi and Trimmer, 1999), but apparently plays a relatively small role in repolarization of individual action potentials when fired at low frequency at normal external $[K^+]$ (Du et al., 2000; Mitterdorfer and Bean, 2002). However, when extracellular $[K^+]$ increases, either by direct experimental manipulation or due to high frequency firing, Kv2.1 channel activity is necessary to maintain action potential integrity (Du et al., 2000).

Our model postulates that the interaction of K356 with an outer vestibule K^+ binding site (Consiglio et al., 2003) combined with the $[K^+]$-dependent change in orientation of this lysine, provides Kv2.1 with the remarkable ability to maintain a cell's K^+ current magnitude when extracellular $[K^+]$ is elevated. Under conditions of rising extracellular $[K^+]$, current magnitude in most neuronal K^+ channels decreases due to the reduction in electrochemical driving force. The unique properties of Kv2.1 serve to oppose the reduction in a cell's net outward current in elevated $[K^+]$. First, the presence of eight outer vestibule lysines limit, by an unknown mechanism, the reduction of outward current in response to reduction in electrochemical driving force (Andalib et al., 2002). Thus, as a result of all passive mechanisms (those that do not include the change in outer vestibule reorientation), elevation of extracellular $[K^+]$ from 0 to 10 mM changes net Kv2.1 macroscopic current by just 7% or less over physiologically relevant membrane potentials (Andalib et al., 2002). (In contrast, currents through the Shaker potassium channel are reduced by as much as 60% due to the change in driving force associated with this change in external $[K^+]$.) Simultaneously, the lysine reorientation mechanism produces an increase in macroscopic current via two mechanisms associated with the shift in channels from the Lys_{in} to Lys_{out} conformation: the increase in single channel conductance demonstrated in this manuscript and an increased rate of channel activation (Consiglio and Korn, 2004). The combined result of all of these Kv2.1 mechanisms is a net increase in outward Kv2.1 current under conditions where outward current through other neuronal K^+ channels is reduced. We propose that this ability to maintain a cell's outward current magnitude in the face of rising external $[K^+]$ is the mechanism by which action potential integrity is maintained in hippocampal neurons under high frequency firing conditions.

We thank Dr. Shin-Ho Chung for performing the HMM analysis. Dr. Chung's contribution to this work was critical, and we are grateful not only for his HMM analysis but also for the education we received in the process.

This work was supported by National Institutes of Health grants NS41090 and NS42563.

Lawrence G. Palmer served as editor.

Submitted: 2 December 2005
Accepted: 14 July 2006

REFERENCES

Andalib, P., M.J. Wood, and S.J. Korn. 2002. Control of outer vestibule dynamics and current magnitude in the Kv2.1 potassium channel. *J. Gen. Physiol.* 120:739–755.

Bao, H., A. Hakeem, M. Henteleff, J.G. Starkus, and M.D. Rayner. 1999. Voltage-insensitive gating after charge-neutralizing mutations in the S4 segment of Shaker channels. *J. Gen. Physiol.* 113:139–151.

Barry, D.M., J.S. Trimmer, J.P. Merlie, and J.M. Nerbonne. 1995. Differential expression of voltage-gated K^+ channel subunits in adult rat heart. Relation to functional K^+ channels? *Circ. Res.* 77:361–369.

Bernèche, S., and B. Roux. 2001. Energetics of ion conduction through the K^+ channel. *Nature.* 414:73–77.

Brelidze, T.I., and K.L. Magleby. 2005. Probing the geometry of the inner vestibule of BK channels with sugars. *J. Gen. Physiol.* 126:105–121.

Brelidze, T.I., X. Niu, and K.L. Magleby. 2003. A ring of eight conserved negatively charged amino acids doubles the conductance of BK channels and prevents inward rectification. *Proc. Natl. Acad. Sci. USA.* 100:9017–9022.

Chapman, M.L., H.M. VanDongen, and A.M. VanDongen. 1997. Activation-dependent subconductance levels in the drk1 K channel suggest a subunit basis for ion permeation and gating. *Biophys. J.* 72:708–719.

Chapman, M.L., H.S. Krovetz, and A.M. VanDongen. 2001. GYGD pore motifs in neighbouring potassium channel subunits interact to determine ion selectivity. *J. Physiol.* 530:21–33.

Chung, S.H., J.B. Moore, L.G. Xia, L.S. Premkumar, and P.W. Gage. 1990. Characterization of single channel currents using digital signal processing techniques based on Hidden Markov Models. *Philos. Trans. R. Soc. Lond. B Biol. Sci.* 329:265–285.

Chung, S.H., V. Krishnamurthy, and J.B. Moore. 1991. Adaptive processing techniques based on hidden Markov models for characterizing very small channel currents buried in noise and deterministic interferences. *Philos. Trans. R. Soc. Lond. B Biol. Sci.* 334:357–384.

Chung, S.H., T.W. Allen, and S. Kuyucak. 2002. Modeling diverse range of potassium channels with Brownian dynamics. *Biophys. J.* 83:263–277.

Consiglio, J.F., and S.J. Korn. 2004. Influence of permeant ions on voltage sensor function in the Kv2.1 potassium channel. *J. Gen. Physiol.* 123:387–400.

Consiglio, J.F., P. Andalib, and S.J. Korn. 2003. Influence of pore residues on permeation properties in the Kv2.1 potassium channel. Evidence for a selective functional interaction of K^+ with the outer vestibule. *J. Gen. Physiol.* 121:111–124.

Du, J., J.H. Tao-Cheng, P. Zerfas, and C.J. McBain. 1998. The K^+ channel, Kv2.1, is apposed to astrocytic processes and is associated with inhibitory postsynaptic membranes in hippocampal and cortical principal neurons and inhibitory interneurons. *Neuroscience.* 84:37–48.

Du, J., L.L. Haak, E. Phillips-Tansey, J.T. Russell, and C.J. McBain. 2000. Frequency-dependent regulation of rat hippocampal somato-dendritic excitability by the K^+ channel subunit Kv2.1. *J. Physiol.* 522:19–31.

Haug, T., D. Sigg, S. Ciani, L. Toro, E. Stefani, and R. Olcese. 2004. Regulation of K^+ flow by a ring of negative charges in the outer pore of BK Ca channels. Part I: Aspartate 292 modulates K^+ conduction by external surface charge effect. *J. Gen. Physiol.* 124:173–184.

Horn, R. 1991. Diffusion of nystatin in plasma membrane is inhibited by a glass-membrane seal. *Biophys. J.* 60:329–333.

Immke, D., and S.J. Korn. 2000. Ion-ion interactions at the selectivity filter. Evidence from K^+-dependent modulation of tetraethylammonium efficacy in Kv2.1 potassium channels. *J. Gen. Physiol.* 115:509–518.

Immke, D., M. Wood, L. Kiss, and S.J. Korn. 1999. Potassium-dependent changes in the conformation of the Kv2.1 potassium channel pore. *J. Gen. Physiol.* 113:819–836.

Jurman, M.E., L.M. Boland, Y. Liu, and G. Yellen. 1994. Visual identification of individual transfected cells for electrophysiology using antibody-coated beads. *Biotechniques.* 17:876–881.

Korn, S.J., and J.G. Trapani. 2005. Potassium channels. *IEEE Trans Nanobioscience.* 4:21–33.

Li, W., and R.W. Aldrich. 2004. Unique inner pore properties of BK channels revealed by quaternary ammonium block. *J. Gen. Physiol.* 124:43–57.

Liu, Y., and R.H. Joho. 1998. A side chain in S6 influences both open-state stability and ion permeation in a voltage-gated K^+ channel. *Pflugers Arch.* 435:654–661.

Lu, T., A.Y. Ting, J. Mainland, L.Y. Jan, P.G. Schultz, and J. Yang. 2001. Probing ion permeation and gating in a K^+ channel with backbone mutations in the selectivity filter. *Nat. Neurosci.* 4:239–246.

MacDonald, P.E., X.F. Ha, J. Wang, S.R. Smukler, A.M. Sun, H.Y. Gaisano, A.M. Salapatek, P.H. Backx, and M.B. Wheeler. 2001. Members of the Kv1 and Kv2 voltage-dependent K^+ channel families regulate insulin secretion. *Mol. Endocrinol.* 15:1423–1435.

MacKinnon, R., and G. Yellen. 1990. Mutations affecting TEA blockade and ion permeation in voltage-activated K^+ channels. *Science.* 250:276–279.

Malin, S.A., and J.M. Nerbonne. 2002. Delayed rectifier K^+ currents, IK, are encoded by Kv2 alpha-subunits and regulate tonic firing in mammalian sympathetic neurons. *J. Neurosci.* 22:10094–10105.

Mitterdorfer, J., and B.P. Bean. 2002. Potassium currents during the action potential of hippocampal CA3 neurons. *J. Neurosci.* 22:10106–10115.

Morais-Cabral, J.H., Y. Zhou, and R. MacKinnon. 2001. Energetic optimization of ion conduction rate by the K^+ selectivity filter. *Nature.* 414:37–42.

Muennich, E.A., and R.E. Fyffe. 2004. Focal aggregation of voltage-gated, Kv2.1 subunit-containing, potassium channels at synaptic sites in rat spinal motoneurones. *J. Physiol.* 554:673–685.

Murakoshi, H., and J.S. Trimmer. 1999. Identification of the Kv2.1 K^+ channel as a major component of the delayed rectifier K^+ current in rat hippocampal neurons. *J. Neurosci.* 19:1728–1735.

Nimigean, C.M., J.S. Chappie, and C. Miller. 2003. Electrostatic tuning of ion conductance in potassium channels. *Biochemistry.* 42:9263–9268.

Perozo, E., D.M. Cortes, and L.G. Cuello. 1999. Structural rearrangements underlying K^+-channel activation gating. *Science.* 285:73–78.

Schoppa, N.E., and F.J. Sigworth. 1998. Activation of Shaker potassium channels. III. An activation gating model for wild-type and V2 mutant channels. *J. Gen. Physiol.* 111:313–342.

So, I., I. Ashmole, N.W. Davies, M.J. Sutcliffe, and P.R. Stanfield. 2001. The K^+ channel signature sequence of murine Kir2.1: mutations that affect microscopic gating but not ionic selectivity. *J. Physiol.* 531:37–50.

Taglialatela, M., J.A. Drewe, G.E. Kirsch, M. De Biasi, H.A. Hartmann, and A.M. Brown. 1993. Regulation of K^+/Rb^+ selectivity and internal TEA blockade by mutations at a single site in K^+ pores. *Pflugers Arch.* 423:104–112.

Trapani, J.G., and S.J. Korn. 2003. Control of ion channel expression for patch clamp recordings using an inducible expression system in mammalian cell lines. *BMC Neurosci.* 4:15.

VanDongen, A.M. 2004. K channel gating by an affinity-switching selectivity filter. *Proc. Natl. Acad. Sci. USA.* 101:3248–3252.

Wood, M.J., and S.J. Korn. 2000. Two mechanisms of K^+-dependent potentiation in Kv2.1 potassium channels. *Biophys. J.* 79: 2535–2546.

Zheng, J., and F.J. Sigworth. 1998. Intermediate conductances during deactivation of heteromultimeric Shaker potassium channels. *J. Gen. Physiol.* 112:457–474.